Current Biology 23, 244–249, February 4, 2013 ©2013 Elsevier Ltd All rights reserved http://dx.doi.org/10.1016/j.cub.2012.12.007

Report

Nanodomain Coupling at an Excitatory Cortical Synapse

Hartmut Schmidt,[1,5,*] Simone Brachtendorf,[1,5] Oliver Arendt,[1] Stefan Hallermann,[1,4] Shimpei Ishiyama,[1] Grit Bornschein,[1] David Gall,[2] Serge N. Schiffmann,[2] Manfred Heckmann,[3] and Jens Eilers[1]
[1]Carl-Ludwig Institute for Physiology, University of Leipzig, 04103 Leipzig, Germany
[2]Laboratoire de Neurophysiologie, Université Libre de Bruxelles, 1070 Bruxelles, Belgium
[3]Institute for Physiology, University of Würzburg, 97070 Würzburg, Germany

Summary

The coupling distance between presynaptic Ca^{2+} influx and the sensor for vesicular transmitter release determines speed and reliability of synaptic transmission [1, 2]. Nanodomain coupling (<100 nm) favors fidelity [1, 2] and is employed by synapses specialized for escape reflexes [3] and by inhibitory synapses involved in synchronizing fast network oscillations [1]. Cortical glutamatergic synapses seem to forgo the benefits of tight coupling [4–6], yet quantitative detail is lacking [2, 7]. The reduced transmission fidelity of loose coupling, however, raises the question whether it is indeed a general characteristic of cortical synapses. Here we analyzed excitatory parallel fiber to Purkinje cell synapses, major processing sites for sensory information [8] and well suited for analysis because they typically harbor only a single active zone [9]. We quantified the coupling distance by combining multiprobability fluctuation analyses, presynaptic Ca^{2+} imaging, and reaction-diffusion simulations in wild-type and calretinin-deficient mice. We found a coupling distance of <30 nm at these synapses, much shorter than at any other glutamatergic cortical synapse investigated to date. Our results suggest that nanodomain coupling is a general characteristic of conventional cortical synapses involved in high-frequency transmission, allowing for dense gray matter packing and cost-effective neurotransmission.

Results

Moderate p_r at PF Terminals

The release probability (p_r) was analyzed at unitary parallel fiber (PF) connections in paired loose-patch/whole-cell recordings between granule cells (GCs) and Purkinje cells (PCs; Figure 1A), under conditions that assured triggering of release by single presynaptic action potentials (APs; Figure 1B and Figure S1A available online). The median excitatory postsynaptic current (EPSC) amplitude (including release failures) was 5.3 pA (interquartile range: 3.6–8.4 pA) and the fraction of synaptic failures was 0.58 (0.48–0.63; n = 16; Figure 1C), indicating that PF synapses operate at moderate quantal size (q) and p_r. Use of a multiple-probability fluctuation analysis (MPFA) of EPSC amplitudes recorded at different extracellular Ca^{2+} concentrations ($[Ca^{2+}]_e$; Figures 1D and 1E), allowed quantifying these parameters. On average (n = 10; Figure 1F), q was 8 pA (5–12 pA) and p_r 0.25 (0.14–0.37) in 2 mM $[Ca^{2+}]_e$, in good agreement with previous reports [10–12]. The binomial parameter N was 2.9 (1.6–4.5), corroborating the notion that AZs of PFs support multivesicular release [9], particularly at high release settings [11].

Spatial Profile of Intraterminal Ca^{2+} Dynamics Estimated from Ca^{2+} Imaging Data

The magnitude of AP-evoked Ca^{2+} transients was quantified in PF terminals of GCs loaded with 200 μM of the low-affinity Ca^{2+} indicator dye Oregon Green 488 BAPTA-6F (Figures 2A and 2B). The fluorescence increase in response to a train of 10 APs (200 Hz) showed little variability within given terminals (Figure 2C), moderate variability between terminals [13], and again little variability when averaging terminals of a given cell (2.1 [1.6–2.2] $\Delta F/F_0$; n = 12 terminals from five cells, Figure 2D). We used the measured Ca^{2+} transients to back calculate spatially resolved Ca^{2+} dynamics with kinetic reaction-diffusion models (Figure 2E and Table S1) differing in the characteristics of endogenous fixed buffers (FBs). FBs with low Ca^{2+} affinity yielded fits that failed to describe the recovery of the Ca^{2+} transients (models "10FB" and "15FB"; Figure 2F) while medium- to high-affinity FBs ("0.1FB" and "1FB") yielded satisfactorily fits as did a model that assumed the absence of FBs ("0FB"). For the latter models, the dye was subsequently removed from the simulations to reflect the conditions in the electrophysiological recordings, and spatially resolved Ca^{2+} dynamics in response to a single AP were deduced. This analysis revealed that calretinin (CR) buffers presynaptic Ca^{2+} depending on the assumed characteristics of the FB and that Ca^{2+} transients drop rapidly with increasing distance from the site of influx with only minor differences between the different Ca^{2+} models (Figure 2G).

The models, which assumed Ca^{2+} influx to occur at a single cluster of channels, represent a functional simplification of the overall topology of presynaptic Ca^{2+} channels. However, they can be expected (and were chosen as such) to predict the maximal local AP-evoked Ca^{2+} increase possible within the terminal, a critical parameter for estimating the coupling distance. Importantly, even with this highly localized Ca^{2+} influx, none of the buffers underwent saturation (for CR, see Figure 2G), which would have led to an underestimation of the Ca^{2+} influx compared to models with more distributed channel topologies.

The Influx-Release Coupling Distance Is in the Nanometer Range

Incorporation of an allosteric five-site release sensor resembling Synaptotagmin 2 (Syt2; model S2a [14]) into the simulation (Figure 3A) allowed calculating release rates at varying coupling distances to the site of influx (Figure 3B). Plotting of the corresponding p_r values against the coupling distance for the three remaining Ca^{2+} models (Figure 3C) revealed

[4]Present address: European Neuroscience Institute Göttingen, 37077 Göttingen, Germany
[5]These authors contributed equally to this work
*Correspondence: hartmut.schmidt@medizin.uni-leipzig.de

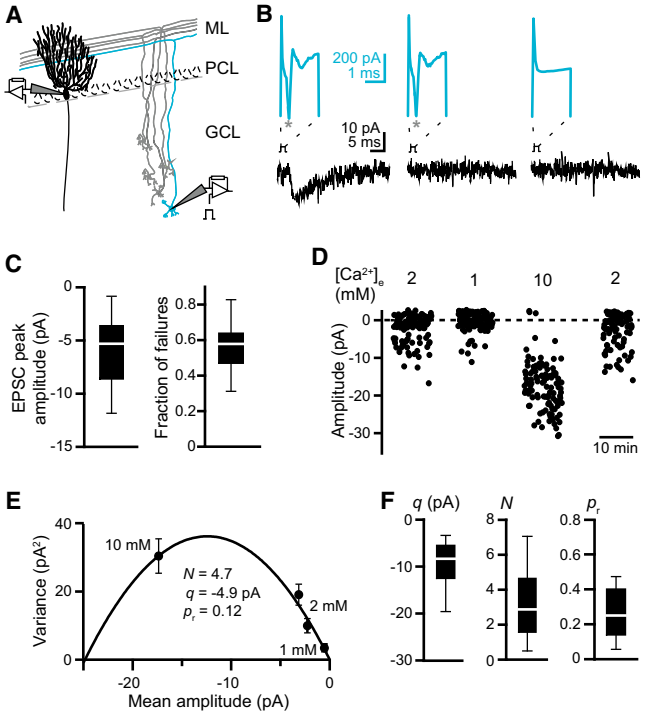

Figure 1. Quantal Analysis Reveals Moderate Release Probability at Unitary PF-PC Synapses

(A) Scheme of experimental arrangement. GCs and PCs were held in the loose-patch and whole-cell configuration, respectively. ML, molecular layer; PCL, Purkinje cell layer; GCL, granule cell layer.

(B) Example of a paired recording showing a synaptic success (left), a release failure (middle), and a subthreshold stimulation (right). Top (blue): currents from the GC (stars denote action currents, initial peaks represent capacitive currents). Bottom: EPSCs from the PC.

(C) Box plots (median and IQR) of EPSC amplitudes and fractions of synaptic failures (n = 16).

(D) Fluctuation analysis of EPSCs amplitudes recorded at the indicated $[Ca^{2+}]_e$ from a single GC-PC connection.

(E) Variance of the amplitudes from (D) plotted versus the corresponding means (with error bars indicating the variance of the variance). The solid line represents a parabolic fit, yielding the quantal size (q), the binominal parameter N, and the average release probability (p_r) at 2 mM $[Ca^{2+}]_e$.

(F) Average quantal parameters (median and IQR, n = 10). Here, as in (C), whiskers show the last data points of the lower and upper quartiles that are still within 1.5 IQR.

See also Figure S1.

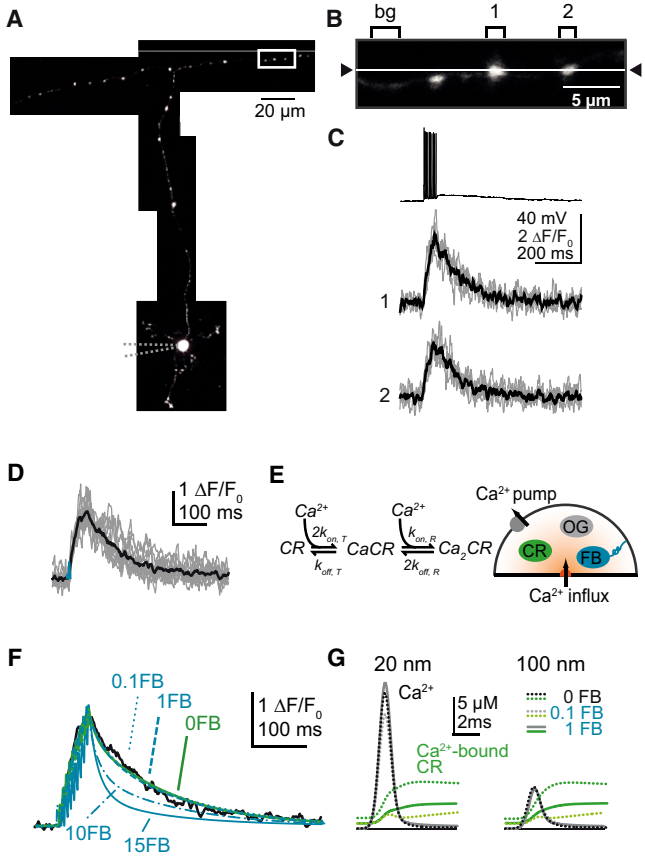

Figure 2. Quantification of Intraterminal Ca^{2+} Dynamics

(A) Two-photon image of a GC filled with the Ca^{2+} indicator dye Oregon Green 488 BAPTA-6F (OG, 200 µM) via a somatic patch-pipette (dashed lines).

(B) PF segment outlined in (A) from which fluorescence signals were recorded (line scan: arrowheads and white line); bg, background; 1 and 2, presumed presynaptic terminals.

(C) Fluorescence signals evoked by 10 APs (200 Hz, top) recorded from the boutons in (B). Individual traces (five recordings) in gray, averages in black.

(D) Fluorescence signals averaged across terminals of a given cell (n = 5 cells, gray) and the corresponding grand average (black).

(E) Scheme of the spatially resolved reaction-diffusion model which included CR, OG, and endogenous fixed buffer (FB).

(F) Averaged fluorescence signal (n = 5 cells, black line) and the simulated fluorescence according to models that differed in the presence and characteristics of the FB (0FB, 0.1FB, 1FB, 10FB, and 15FB). Note that the models 10FB and 15FB failed to reproduce the measured transient.

(G) Expected transients of free Ca^{2+} (black) and of absolute Ca^{2+} bound to CR (green) at 20 and 100 nm distance from the site of Ca^{2+} influx for the indicated Ca^{2+} models (solid, dotted and dashed lines).

See also Figure S2 and Table S1.

exponential dependencies with length constants in the range of 20 to 40 nm. p_r values obtained from the MPFA (Figure 1F) were best explained by a coupling distance of 10 to 35 nm (for the median p_r value; 5–42 nm for the interquartile range [IQR] of p_r values; thick segments in Figure 3C). We tested variations of the release model, in which release either occurred only from the fully occupied sensor (model S2b and S2c [15, 16]), in which a fraction (0.2) of CR was immobilized by binding to Ca^{2+} channels [17], or in which the temporal profile of the Ca^{2+} influx was varied to cover the range of conceivable AP widths (Figure S3). All of these variations gave similar results, particularly with respect to the short coupling distance. Notably, the estimated distance represents an upper limit because the cluster model, with Ca^{2+} influx modeled as a single point source, generated the largest possible Ca^{2+} concentration close to a putative sensor. More distributed channel topologies would generate spatially broadened signals with lower peak Ca^{2+} concentrations, which, in turn, would require even shorter coupling to be consistent with the measured release probability.

In order to substantiate the prediction of nanodomain coupling, we performed experiments in which the effect of the exogenous buffers EGTA and BAPTA on EPSCs evoked by tract stimulation was assessed (Figures 3D and 3E). Bath application of membrane permeable BAPTA (BAPTA-AM; 10 µM, 30 min) led to a significant reduction of the EPSC amplitudes. EGTA-AM (10 µM, 30 min), on the other hand, did not affect EPSC amplitudes compared to control. The finding that EGTA, a buffer with higher Ca^{2+} affinity but slower

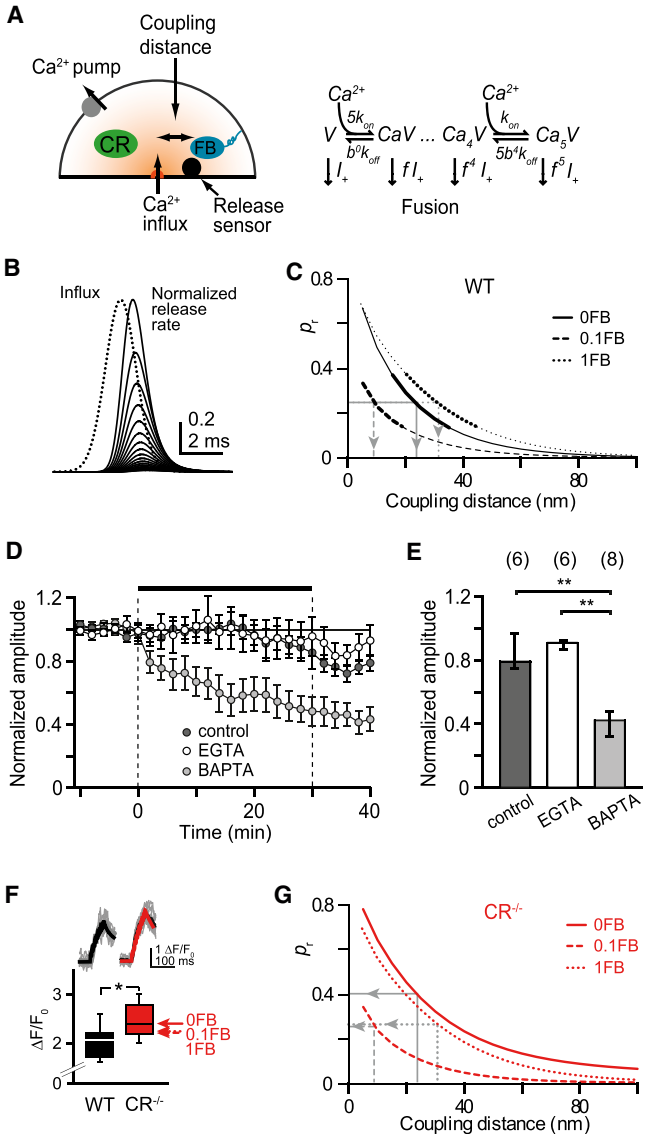

Figure 3. Nanodomain Influx-Release Coupling

(A) Reaction-diffusion model (cf. Figure 2E) extended by an allosteric release sensor (V) positioned at varying coupling distance from the site of Ca^{2+} influx.

(B) Release rates (solid lines) at increasing coupling distances (5 to 100 nm in 5 nm increments), normalized to the peak rate at 5 nm. The dotted line indicates the self-normalized Ca^{2+} influx.

(C) Calculated p_r at different coupling distances for simulations with a medium- or high-affinity FB (1FB and 0.1FB, dotted and dashed lines, respectively) or without an FB (0FB, solid line). The gray lines indicate the experimentally determined p_r (0.25; cf. Figure 1F) and the corresponding coupling distances predicted by the different simulations. The thickened segments of the curves indicate the range covered by the interquartile range of p_r values.

(D) Change in amplitude of EPSCs evoked by tract stimulation upon bath application of EGTA-AM or BAPTA-AM (both 10 μM, dissolved in 0.1% DMSO) or sham application (0.1% DMSO, "control"; mean ± SEM, n = 6, 8, and 6, respectively). EPSC were evoked every 5 s, amplitudes were binned (2 min) and normalized to the average of baseline period.

(E) Average reduction of EPSC amplitude in the 10 min period after EGTA-AM, BAPTA-AM, or sham application (median ± IQR; **p = 0.08 for control versus BAPTA and p = 0.003 for EGTA versus BAPTA, respectively. p = 0.818 for control versus EGTA).

(F) Top: Initial phase of AP-evoked Ca^{2+} transients in WT (left, cf. Figure 2F) and $CR^{-/-}$ PF boutons (right). Signals from individual cells in gray (n = 5 and 5, WT and $CR^{-/-}$, respectively). The grand average and the prediction of model "0FB" are shown in dark gray and black for the WT and in black and red for the $CR^{-/-}$. Bottom: $\Delta F/F_0$ values in WT (median and IQR; n = 12 from 5 cells, black) and $CR^{-/-}$ boutons (red; n = 13, 5 cells; *p = 0.009). Whiskers show the last data points of the lower and upper quartiles that are still within 1.5 IQR. The red arrows indicate the amplitude predicted by the indicated models.

(G) As in (C) but for $CR^{-/-}$ terminals. The gray lines indicate the p_r values predicted by the different models for $CR^{-/-}$ synapses based on the coupling distance estimated from the WT (Figure 3C). Note that only model 0FB predicts an increase in p_r in $CR^{-/-}$ synapses.

See also Figure S3 and Table S1.

binding kinetics compared to BAPTA [2], did not affect release supports the notion of nanodomain coupling [4, 5].

Confirmation of Model Predictions in $CR^{-/-}$ Mice

Bath application of AM buffers leaves their intracellular concentration rather ill defined. Our simulations indicate that CR, the major endogenous Ca^{2+} buffer of GCs [18], significantly buffers Ca^{2+} in the terminal (Figure 2G). We therefore repeated our experiments in mice deficient for CR [18] to test for the effect of this endogenous buffer on release. Ca^{2+} transients in $CR^{-/-}$ terminals were significantly larger (median 2.4 $\Delta F/F_0$, IQR 2.2–2.8, n = 13, p = 0.009) than in the wild-type (WT; Figure 3F) and well predicted by the simulations. The data were best described by model "0FB," i.e., in the absence of a FB, but incorporating a FB (model 0.1FB and 1FB) also produced reasonable result (Figure 3F).

Feeding of the corresponding Ca^{2+} dynamics into the release model yielded distinct predictions for p_r in $CR^{-/-}$ synapses (Figure 3G). In the presence of either medium or high-affinity FBs (1FB and 0.1FB, respectively), the simulations predicted no significant effect on p_r (Figure 3G). On the other hand, the 0FB model predicted a p_r value almost twice as high as in the WT (Figure 3G).

Paired recordings of unitary $CR^{-/-}$ PF connections showed a significant decrease in the fraction of synaptic failures (0.38; 0.26–0.55; p = 0.041, data not shown, cf. Figure 1C), indicating that p_r was increased in $CR^{-/-}$ connections. Indeed, MPFA of $CR^{-/-}$ connections (Figures 4A and 4B) revealed that neither q (9 pA, 7–12 pA, n = 8, p = 0.894) nor N (2.7; 1.6–4.4, p = 0.965) was different from the WT but that p_r was significantly increased to 0.41 (0.35–0.60, p = 0.046). This value excellently agreed with the prediction of the model that did not include a FB but in which CR was the dominating buffer (model "0FB"; Figure 4C, cf. Figure 3G). With model 0FB, the coupling distance was estimated to be 24 nm.

In a next step, an analytical steady-state solution to the linearized reaction diffusion problem of model 0FB was analyzed [1]. The linearization of the single cluster of Ca^{2+} channels overlapped well with the estimates of the full reaction diffusion model (Figure S4A). Also for the linearized model, the observed difference in p_r values between WT and $CR^{-/-}$ synapses indicated a coupling distance in the range of 25 nm. Shorter or longer distance would predict effects of CR on p_r that are inconsistent with the experimental data. The linearization allowed analysis of more-distributed channel topologies in which the release sensor couples to the center of a larger array of Ca^{2+} channels (Figure S4B). Increase of the spatial extent of the array required shorter coupling distances. Notably, channel topologies wider than 25 nm required coupling distances significantly shorter than 25 nm (Figure S4B).

In the cerebellar molecular layer both Syt1 and Syt2 are expressed [19]. While it is unclear whether GC terminals

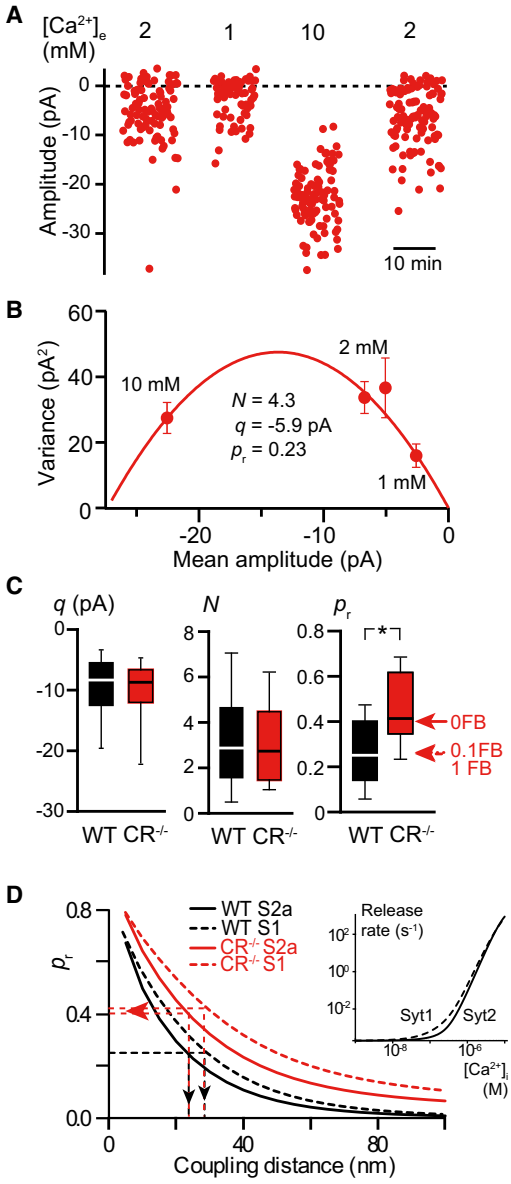

Figure 4. Data from $CR^{-/-}$ Synapses Confirm the Model Predictions

(A and B) MPFA from a unitary $CR^{-/-}$ connection. The error bars denote the variance of the variance.

(C) Comparison of quantal parameters in WT (cf. Figure 1F) and $CR^{-/-}$ terminals (n = 8; *p = 0.046). The red arrows indicate the p_r value predicted by the models 0FB, 0.1FB, and 1 FB (cf. Figure 3G).

(D) Comparison of different release sensor models representing synaptogamin 1 and synaptogamin 2 (S1 and S2a, respectively). The Ca^{2+} dynamics were simulated according to model 0FB. The straight dashed lines indicate p_r determined in the WT and the predicted coupling distances (black), as well as the predicted p_r for $CR^{-/-}$ synapses. Note that both sensor models predict similar effects for $CR^{-/-}$ synapses and similar coupling distances. The inset shows the Ca^{2+} dependence of the release rates of the two sensors.

See also Figure S4.

express just one of the two or both isoforms (ibid.), there is evidence that Syt2 is the predominant isoform at the age of animals we used in our study [20]. Compared to Syt2, Syt1 differs slightly in its release characteristics at low $[Ca^{2+}]$, with Syt2 being optimized for phasic release [21]. We therefore tested in as much the prediction of nanodomain coupling is affected by assuming that PFs employ only Syt1 for transmission. Importantly, the sensor resembling Syt1 predicted a similar increase in p_r in CR compared to the WT (Figure 4D). The predicted coupling distance was slightly larger (29 nm) than with a Syt2-like sensor (24 nm) but still clearly in the nanodomain range.

Discussion

We report here that PF terminals, very probably the most numerous synapses in the brain, operate at a coupling distance of <30 nm between Ca^{2+} influx and release sensor. While such tight coupling has been reported for fast spiking hippocampal and cerebellar interneurons [1, 2], where it contributes to the speed and reliability of inhibition [1], it was unexpected for cortical excitatory synapses [2, 4–6, 22]. Our data indicate that glutamatergic PF synapses exploit the benefits of tight coupling, too, in order to allow for reliable transmission of their characteristic high-rate burst activity evoked by sensory stimulation [8].

We modified the established approach of analyzing effects of added, exogenous buffer on transmitter release [3] by quantifying the effect of CR, the main endogenous buffer of GCs [18]. CR has complex binding kinetics [23]: EF hands I–IV represent two pairs of binding sites with kinetics similar to EGTA or, upon binding of the first calcium ion, to BAPTA. In view of these properties and its assumed submillimolar concentration, it may appear surprising that CR strongly affects p_r at a synapse with nanodomain coupling, an effect for which tens of millimolar of fast exogenous buffers are needed at the giant squid synapse [3] or at cortical GABAergic synapses [1]. Two reasons, however, account for the relatively high effectiveness of CR at PF synapses. First, as pointed out by Faas et al. [23], compared to EGTA and BAPTA, CR has a low resting Ca^{2+} occupancy, which provides an optimal buffer capacity for AP-mediated Ca^{2+} influx. Second, the Ca^{2+} transients at the release site of PFs reached peak values of 20–25 μM, similar to the range estimated for the calyx of Held [16] but much lower than those assumed to trigger release at other nanodomain synapses [1, 3]. The former transients are within the range in which release depends supralinearly on Ca^{2+} [14, 21, 24], while the latter can be expected to saturate release [14]. Importantly, the relatively weak buffering by CR (10%–15% differences in Ca^{2+} transients of the WT versus $CR^{-/-}$, Figure 3F) explains well the 40%–50% differences in p_r (Figure 4C), indicating significant nanodomain buffering by CR.

For the influx-release model, we assumed that release of a given vesicle is triggered by a neighboring single cluster of Ca^{2+} channels. This scenario appears to be not unlikely, considering the prevalence and functional contributions of different Ca^{2+} channel subtypes [24], their intraterminal distribution [25], and their potentially low open probability [26]. Unfortunately, for typical cortical synapses, the latter parameter has not been determined. While hippocampal mossy fiber boutons operate at a high open probability [27], low probabilities (0.1–0.2) have been reported for the calyx of Held [28] and other synapses [e.g., 26]. High-probability activation of Ca^{2+} channels would speak in favor of more distributed Ca^{2+} influx [25]. However, the corresponding simulations still predict a rather small, nanodomain cluster of channels (width <60 nm) and an ultrashort coupling distance of fully primed vesicles to its center (Figure S4B). A low-probability activation of Ca^{2+} channels, on the other hand, would be in accord with

the notion that nanodomain coupling allows a single Ca^{2+} channel to trigger release [29, 30]. The small number of docked vesicles at PF terminals [9], the comparable number of Ca^{2+} channels [25] and our estimate of the coupling distance would be in agreement with this scenario.

Tight nanodomain coupling in excitatory synapses has previously been found only in highly specialized synapses of the peripheral nervous system and the brain stem [2, 7] but not in conventional cortical boutons. We suggest that in addition to optimizing synaptic signaling [1, 2], nanodomain coupling allows for smaller boutons by drastically reducing the demands on Ca^{2+} signaling and in turn the size of presynaptic compartments [31]. Thus, tight coupling may be a prerequisite for the dense packing of cortical synapses in mammalian cortices.

Experimental Procedures

Patch-clamp recordings were performed at 20°C–22°C on acute slices prepared from 21- to 27-day-old C57BL/6 or $CR^{-/-}$ mice [18]. Postsynaptic PCs were held in the whole-cell configuration, and presynaptic GCs were depolarized in the loose-patch configuration (unitary connections) or activated by tract stimulation. Quantal synaptic parameters were estimated from unitary EPSCs recorded at different $[Ca^{2+}]_e$ by a multiple-probability fluctuation analysis. Ca^{2+} imaging experiments were performed on GCs dialyzed in the whole-cell configuration with a Ca^{2+}-sensitive indicator dye. Ca^{2+} transients in response to somatically induced APs were recorded in line scans (500 Hz resolution) with a custom-build two-photon microscope and expressed as background-corrected $\Delta F/F_0$. Ca^{2+} dynamics and transmitter release were simulated by numerical solving of a system of ordinary differential equations placed in concentric hemi-shells of 5 nm thickness. The shells were coupled by diffusion of all reactants. AP-mediated Ca^{2+} influx was placed in the central shell. Ca^{2+} binding was simulated by second order kinetics, except for CR, for which cooperativity was implemented. A surface-based extrusion mechanism was balanced by a Ca^{2+} leak to generate a resting $[Ca^{2+}]_i$ of 45 nM. An allosteric sensor model for vesicle fusion [14] was placed at varying distances from the influx.

Unless otherwise stated, average data are given as median and IQR. Whiskers in box plots show the last data points of the lower and upper quartiles that are still within 1.5 IQR. In mean versus variance plots (Figures 1E and 4B), variance data are given as mean and variance. The Wilcoxon-Mann-Whitney two-sample rank-sum test was used for comparisons. Full methods are available in the Supplemental Experimental Procedures.

Supplemental Information

Supplemental Information includes Supplemental Experimental Procedures, four figures, and one table and can be found with this article online at http://dx.doi.org/10.1016/j.cub.2012.12.007.

Acknowledgments

We thank Gudrun Bethge for technical assistance and Robert Kittel for comments on the manuscript. This work was supported by grants to J.E. and H.S. (DFG, EI 342/4), to S.H. (DFG, HA 6386/1), to S.N.S. and D.G. (FRS-FNRS; QEMF, FMRE; ARC, CFWB), and to M.H. (DFG, HE 2621/4 and SFB 581).

Received: November 4, 2012
Revised: December 6, 2012
Accepted: December 7, 2012
Published: December 27, 2012

References

1. Bucurenciu, I., Kulik, A., Schwaller, B., Frotscher, M., and Jonas, P. (2008). Nanodomain coupling between Ca^{2+} channels and Ca^{2+} sensors promotes fast and efficient transmitter release at a cortical GABAergic synapse. Neuron *57*, 536–545.
2. Eggermann, E., Bucurenciu, I., Goswani, S.P., and Jonas, P. (2011). Nanodomain coupling between Ca^{2+} channels and sensors of exocytosis at fast mammalian synapses. Nat. Rev. Neurosci. *13*, 7–21.
3. Adler, E.M., Augustine, G.J., Duffy, S.N., and Charlton, M.P. (1991). Alien intracellular calcium chelators attenuate neurotransmitter release at the squid giant synapse. J. Neurosci. *11*, 1496–1507.
4. Rozov, A., Burnashev, N., Sakmann, B., and Neher, E. (2001). Transmitter release modulation by intracellular Ca^{2+} buffers in facilitating and depressing nerve terminals of pyramidal cells in layer 2/3 of the rat neocortex indicates a target cell-specific difference in presynaptic calcium dynamics. J. Physiol. *531*, 807–826.
5. Ohana, O., and Sakmann, B. (1998). Transmitter release modulation in nerve terminals of rat neocortical pyramidal cells by intracellular calcium buffers. J. Physiol. *513*, 135–148.
6. Nadkarni, S., Bartol, T.M., Stevens, C.F., Sejnowski, T.J., and Levine, H. (2012). Short-term plasticity constrains spatial organization of a hippocampal presynaptic terminal. Proc. Natl. Acad. Sci. USA *109*, 14657–14662.
7. Augustine, G.J., Santamaria, F., and Tanaka, K. (2003). Local calcium signaling in neurons. Neuron *40*, 331–346.
8. Chadderton, P., Margrie, T.W., and Häusser, M. (2004). Integration of quanta in cerebellar granule cells during sensory processing. Nature *428*, 856–860.
9. Xu-Friedman, M.A., Harris, K.M., and Regehr, W.G. (2001). Three-dimensional comparison of ultrastructural characteristics at depressing and facilitating synapses onto cerebellar Purkinje cells. J. Neurosci. *21*, 6666–6672.
10. Sims, R.E., and Hartell, N.A. (2005). Differences in transmission properties and susceptibility to long-term depression reveal functional specialization of ascending axon and parallel fiber synapses to Purkinje cells. J. Neurosci. *25*, 3246–3257.
11. Foster, K.A., Crowley, J.J., and Regehr, W.G. (2005). The influence of multivesicular release and postsynaptic receptor saturation on transmission at granule cell to Purkinje cell synapses. J. Neurosci. *25*, 11655–11665.
12. Valera, A.M., Doussau, F., Poulain, B., Barbour, B., and Isope, P. (2012). Adaptation of granule cell to Purkinje cell synapses to high-frequency transmission. J. Neurosci. *32*, 3267–3280.
13. Brenowitz, S.D., and Regehr, W.G. (2007). Reliability and heterogeneity of calcium signaling at single presynaptic boutons of cerebellar granule cells. J. Neurosci. *27*, 7888–7898.
14. Lou, X., Scheuss, V., and Schneggenburger, R. (2005). Allosteric modulation of the presynaptic Ca^{2+} sensor for vesicle fusion. Nature *435*, 497–501.
15. Schneggenburger, R., and Neher, E. (2000). Intracellular calcium dependence of transmitter release rates at a fast central synapse. Nature *406*, 889–893.
16. Bollmann, J.H., Sakmann, B., and Borst, J.G. (2000). Calcium sensitivity of glutamate release in a calyx-type terminal. Science *289*, 953–957.
17. Christel, C.J., Schaer, R., Wang, S., Henzi, T., Kreiner, L., Grabs, D., Schwaller, B., and Lee, A. (2012). Calretinin regulates Ca^{2+}-dependent inactivation and facilitation of $Ca_v2.1$ Ca^{2+} channels through a direct interaction with the $\alpha_1$2.1 subunit. J. Biol. Chem. *287*, 39766–39775.
18. Schiffmann, S.N., Cheron, G., Lohof, A., d'Alcantara, P., Meyer, M., Parmentier, M., and Schurmans, S. (1999). Impaired motor coordination and Purkinje cell excitability in mice lacking calretinin. Proc. Natl. Acad. Sci. USA *96*, 5257–5262.
19. Fox, M.A., and Sanes, J.R. (2007). Synaptotagmin I and II are present in distinct subsets of central synapses. J. Comp. Neurol. *503*, 280–296.
20. Berton, F., Iborra, C., Boudier, J.A., Seagar, M.J., and Marquèze, B. (1997). Developmental regulation of synaptotagmin I, II, III, and IV mRNAs in the rat CNS. J. Neurosci. *17*, 1206–1216.
21. Kochubey, O., and Schneggenburger, R. (2011). Synaptotagmin increases the dynamic range of synapses by driving Ca^{2+}-evoked release and by clamping a near-linear remaining Ca^{2+} sensor. Neuron *69*, 736–748.
22. Meinrenken, C.J., Borst, J.G., and Sakmann, B. (2002). Calcium secretion coupling at calyx of held governed by nonuniform channel-vesicle topography. J. Neurosci. *22*, 1648–1667.
23. Faas, G.C., Schwaller, B., Vergara, J.L., and Mody, I. (2007). Resolving the fast kinetics of cooperative binding: Ca^{2+} buffering by calretinin. PLoS Biol. *5*, e311.
24. Mintz, I.M., Sabatini, B.L., and Regehr, W.G. (1995). Calcium control of transmitter release at a cerebellar synapse. Neuron *15*, 675–688.

25. Kulik, Á., Nakadate, K., Hagiwara, A., Fukazawa, Y., Luján, R., Saito, H., Suzuki, N., Futatsugi, A., Mikoshiba, K., Frotscher, M., and Shigemoto, R. (2004). Immunocytochemical localization of the α_{1A} subunit of the P/Q-type calcium channel in the rat cerebellum. Eur. J. Neurosci. *19*, 2169–2178.
26. King, J.D., Jr., and Meriney, S.D. (2005). Proportion of N-type calcium current activated by action potential stimuli. J. Neurophysiol. *94*, 3762–3770.
27. Bischofberger, J., Geiger, J.R., and Jonas, P. (2002). Timing and efficacy of Ca^{2+} channel activation in hippocampal mossy fiber boutons. J. Neurosci. *22*, 10593–10602.
28. Sheng, J., He, L., Zheng, H., Xue, L., Luo, F., Shin, W., Sun, T., Kuner, T., Yue, D.T., and Wu, L.G. (2012). Calcium-channel number critically influences synaptic strength and plasticity at the active zone. Nat. Neurosci. *15*, 998–1006.
29. Weber, A.M., Wong, F.K., Tufford, A.R., Schlichter, L.C., Matveev, V., and Stanley, E.F. (2010). N-type Ca^{2+} channels carry the largest current: implications for nanodomains and transmitter release. Nat. Neurosci. *13*, 1348–1350.
30. Graydon, C.W., Cho, S., Li, G.L., Kachar, B., and von Gersdorff, H. (2011). Sharp Ca^{2+} nanodomains beneath the ribbon promote highly synchronous multivesicular release at hair cell synapses. J. Neurosci. *31*, 16637–16650.
31. Holderith, N., Lorincz, A., Katona, G., Rózsa, B., Kulik, A., Watanabe, M., and Nusser, Z. (2012). Release probability of hippocampal glutamatergic terminals scales with the size of the active zone. Nat. Neurosci. *15*, 988–997.